Organic & Biomolecular Chemistry

Accepted Manuscript

ROYAL SOCIETY OF CHEMISTRY

www.rsc.org/obc

Cite this: DOI: 10.1039/c0xx00000x

www.rsc.org/xxxxxx

ARTICLE TYPE

Thiophene-Based Dyes for Probing Membranes

Ismael López-Duarte,[a] Phoom Chairatana,[a] Yilei Wu,[b] Javier Pérez-Moreno,[c] Philip M. Bennett,[a] James E. Reeve,[a] Igor Boczarow,[a] Wojciech Kaluza,[a] Neveen A. Hosny,[b] Samuel D. Stranks,[d] Robin J. Nicholas,[d] Koen Clays,*[c] Marina K. Kuimova*[b] and Harry L. Anderson*[a]

Received (in XXX, XXX) Xth XXXXXXXXX 20XX, Accepted Xth XXXXXXXXX 20XX
DOI: 10.1039/b000000x

We report the synthesis of four new cationic dipolar push-pull dyes, together with an evaluation of their photophysical and photobiological characteristics pertinent to imaging membranes by fluorescence and second harmonic generation (SHG). All four dyes consist of an *N*,*N*-diethylaniline electron-donor conjugated to a pyridinium electron-acceptor via a thiophene bridge, with either vinylene (-CH=CH-) or ethynylene (-C≡C-) linking groups, and with either singly-charged or doubly-charged pyridinium terminals. The absorption and fluorescence behavior of these dyes were compared to a commercially available fluorescent membrane stain, the styryl dye **FM4-64**. The hyperpolarizabilities of all dyes were compared using hyper-Rayleigh scattering at 800 nm. Cellular uptake, localization, toxicity and phototoxicity were evaluated using tissue cell cultures (HeLa, SK-OV-3 and MDA-231). Replacing the central alkene bridge of **FM4-64** with a thiophene does not substantially change the absorption, fluorescence or hyperpolarizability, whereas changing the vinylene-links to ethynylenes shifts the absorption and fluorescence to shorter wavelengths, and reduces the hyperpolarizability by about a factor of two. SHG and fluorescence imaging experiments in live cells showed that the doubly-charged thiophene dyes localize in plasma membranes, and exhibit lower internalization rates compared to **FM4-64**, resulting in less signal from the cell cytosol. At a typical imaging concentration of 1 μM, the doubly-charged dyes showed no significant light or dark toxicity, whereas the singly-charged dyes are phototoxic even at 0.5 μM. The doubly-charged dyes showed phototoxicity at concentrations greater than 10 μM, although they do not generate singlet oxygen, indicating that the phototoxicity is type I rather than type II. The doubly-charged thiophene dyes are more effective than **FM4-64** as SHG dyes for live cells.

Introduction

Many dyes have been developed for probing the structure and functions of complex biological systems, yet there is an urgent need for new dyes to exploit recent advances in optical imaging techniques.[1] Linear optical microscopy, and in particular fluorescence microscopy, is a powerful tool for imaging live cells and tissues with minimal structural or chemical invasion. However, there are several drawbacks inherent to this technique, such as photodamage, photobleaching and shallow penetration depths, which can be overcome by utilizing multiphoton processes.[2] Nonlinear optical (NLO) microscopy has emerged as a promising alternative to one-photon fluorescence microscopy for non-invasive 3D imaging of biological tissues.[3] The most common forms of NLO microscopy rely on two nonlinear phenomena: Two-photon excited fluorescence (TPEF) and second harmonic generation (SHG). These techniques both use wavelengths of incident light in the near-infrared (NIR) range to achieve deeper penetration through biological tissues and reduce scattering. Second harmonic imaging microscopy (SHIM) utilizes a NLO effect whereby chromophores in a non-centrosymmetric environment generate scattered light of twice the incident frequency.[4,5] This technique yields information on interfaces and membranes, of a type which is not provided by fluorescence microscopy. Moreover, photobleaching and other photodamage can be avoided during SHIM since, in principle, population of excited states is not required for signal generation.[5] In recent years, SHIM has also become an attractive tool for mapping electrical activity in complex neuronal systems.[4]

In order to be useful as SHG membrane probes, a chromophore must be non-centrosymmetric, exhibit a high molecular first hyperpolarizability, β, and insert non-centrosymmetrically into the lipid bilayer. Currently, most membrane probes used for SHIM consist of amphiphilic push-pull chromophores in which aromatic electron-donors and acceptors are linked by π-conjugated polyene bridges, to ensure effective coupling between the donor and acceptor groups.[5] Although increasing the polyenic chain-length is a good strategy for enhancing the molecular first hyperpolarizability,[6] extended polyenes suffer from poor chemical and photochemical stability.[7] Thus there is a growing interest in new amphiphilic push-pull membrane probes based on other π-conjugated units. We recently

reported that porphyrin dyes can be engineered for SHG imaging of cell membranes,[8] while Andraud and co-workers have used fluorethynyl π-conjugated bridge to construct probes for TPEF and SHG imaging.[9] Other promising new chromophores in this field include dyes based on benzothiazolium salts[10] and carbazoles.[11]

In parallel with the engineering of new NLO dyes for biological multiphoton imaging, there have been rapid advances in the design of molecular NLO materials for telecommunications and photonics applications.[12] Chromophores with large hyperpolarizabilities and high chemical stability are needed for frequency-doublers, electro-optic switches and modulators. There is substantial overlap between the molecular design requirements in these two areas. Thiophene-based donor-π-acceptor (D-π-A) chromophores are among the most promising NLO dyes for electro-optic applications, because of their large β values and chemical stability,[13] however thiophene-based dyes have received less attention in biological contexts.[7,14]

Here, we report the synthesis and characterization of four thiophene-based push-pull dyes **1a**, **1b**, **2a** and **2b** (Schemes 1 and 2). We compare the optical and biological properties of these new dyes with those of the widely used dye **FM4-64**, which is available commercially. **FM4-64** was developed by Fei Mao and coworkers as a membrane-selective fluorescent probe.[15] It is one of a range of "FM-dyes", which have been employed extensively for both fluorescence and SHG imaging of membranes to study vesicle trafficking,[15] organelle organization in live cells[16] or change in transmembrane potential in neurons.[17]

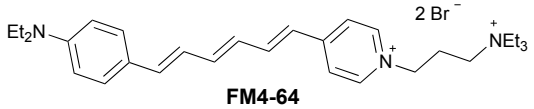

FM4-64

The original motivation for the work presented here was to explore the consequences of replacing the central vinylene core of **FM4-64** with a thiophene unit, and to investigate how this modification in the molecular structure would alter the performance of the dye as a multiphoton membrane probe. We also sought to compare the behavior of dyes with acetylenic (-C≡C-) and olefinic (-CH=CH-) bridges, and to test compounds with singly- and doubly-charged pyridinium head groups. Here we present the synthesis, linear optical properties, hyperpolarizabilities and cytotoxicities of these thiophene-based dyes, together with results from *in vitro* TPEF and SHG imaging in live cells.

Results and discussion

Synthesis

Compounds **1a/b** and **2a/b** share a common structural motif which employs a thiophene unit as the π-conjugated bridge. The 4-(diethylamino)phenyl substituent is used as an electron-donor, while a pyridinium group acts as the electron-acceptor. The positively charged head-group prevents the dye from diffusing through the membrane by anchoring it in the aqueous phase, thus causing the dye to align in one direction in the cell plasma membrane. This is crucial for SHG, which requires that the molecules be ordered in a non-centrosymmetric environment. The polar head group also increases the solubility of the dye in water, which is desirable for imaging live cells. The synthesis of both dyes **1a** and **1b** was carried out by Knoevenagel condensation of the thiophene aldehyde **3** with the corresponding pyridinium salt **4a,b**, by adapting the procedure of Wuskell et al.[7] (Scheme 1).

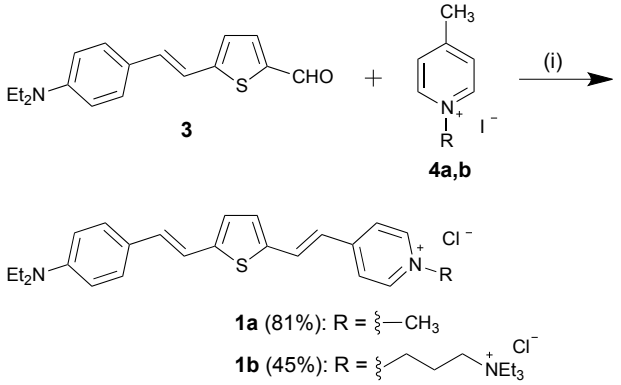

Scheme 1 Synthesis of dyes **1a,b**: (i) **4a** or **4b**, pyrrolidine, EtOH, 20 °C.

The synthesis of the alkyne-linked thiophene dyes **2a,b** was achieved by a different strategy, based on the preparation of the precursor pyridine derivative **6**, followed by *N*-alkylation with a two alternative head groups. Compound **5** underwent deprotection and palladium-catalyzed Sonogashira coupling with 4-iodopyridine, leading to the neutral pyridine chromophore **6**. Dye **2a** was prepared by *N*-alkylation of pyridine **6** with methyl iodide in THF at room temperature. The product crystallized from the reaction mixtures as a dark red precipitate, without the need for further purification.

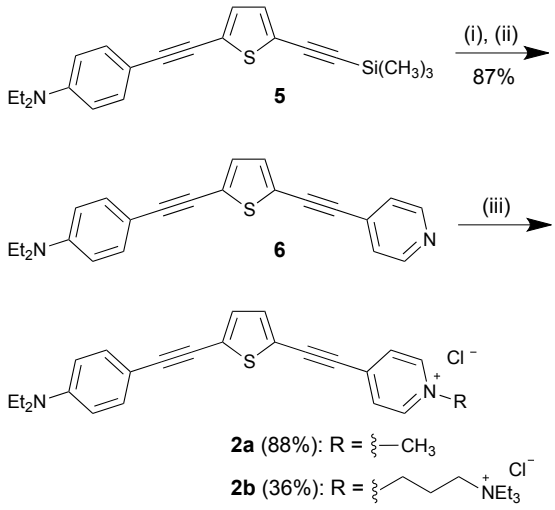

Scheme 2 Synthesis of dyes **2a,b**: (i) K_2CO_3, 3:1 THF/MeOH, 20 °C; (ii) 4-iodopyridine, $Pd_2(dba)_3$, PPh_3, CuI, toluene, *i*-Pr_2NH, 20 °C; (iii) MeI, THF, overnight or (3-iodopropyl)triethylammonium iodide, DMSO/benzonitrile, 75 °C.

Preparation of **2b** was more difficult due to the low solubility of the (3-iodopropyl)triethylammonium iodide salt. A mixture of DMSO/benzonitrile (1:1) proved to be the most suitable solvent for the quarternization. After column chromatography, eluting with a mixture of 7:2:1 MeOH:NH_4Cl (0.2 M aq.):$MeNO_2$,[18] compound **2b** was isolated in 36% yield as a red waxy solid. The

doubly-charged vinylene-linked compounds, **FM4-64** and **1b** are readily soluble in water, whereas the other compounds only dissolve in water in the presence of small amounts of organic solvents, such as DMSO or methanol.

Linear Optical Properties

The absorption and emission spectra of **FM4-64**, **1a,b** and **2a,b** in chloroform are displayed in Fig. 1a. As expected, the absorption maxima of derivatives **1a,b** are red-shifted relative to those of **2a,b**, reflecting the more efficient conjugation through vinylene bridges. All the dyes exhibit fluorescence at substantially longer wavelengths than absorption. The large Stokes shifts ($\Delta\tilde{\nu} \approx 4000$–$6000$ cm^{-1}) should allow for convenient filtering of excitation from emission during fluorescence imaging.

It is well known that styryl dyes (e.g. **FM4-64**) and several non-covalent nucleic acid stains (e.g. DAPI, TO-PRO-3, propidium iodide) are essentially non-fluorescent in water, and only fluoresce when in hydrophobic environments, when intercalated into membranes or DNA.[19] This change in fluorescence intensity is an advantage since it avoids the need for washing steps, to remove unbound dye prior to imaging. Similar behavior is observed for dyes **1a,b**, which exhibit no significant emission in aqueous solutions. When the surfactant polysorbate-80 is added to aqueous solutions of **FM4-64** and **1b** (1 μM), both dyes show a strong fluorescence increase (*ca.* 10-fold, Fig S11) and a blue shift of the emission maxima, which is consistent with their localization in the hydrophobic environment of the polysorbate-80 micelles.[20]

Like most styryl dyes, all these compounds exhibit negative solvatochromism in absorption, and positive solvatochromism in emission,[21] as seen for the spectra of **FM4-64** (Fig. 1c), **1b** (Fig. 1d) and **2b** (Fig. S10) in toluene, chloroform, dichloromethane, acetonitrile, methanol and water. The negative solvatochromism in the absorption spectra appears to be complicated by aggregation effects in toluene, whereas the emission spectra show clear positive solvatochromism, as illustrated by the linear correlation with Reichardt's E_T polarity parameter[22] (Fig. 1b). This solvatochromism results in a dramatic increase in the Stokes shift in more polar solvents such as acetonitrile, methanol and water. The extreme reduction of the π-π* gap in water probably contributes to the low fluorescence quantum yield in this solvent. The similarity between the absorption and emission spectra of **FM4-64** and **1b** is remarkable. These two compounds display almost identical solvatochromism (Fig. 1b–d), indicating that their first excited states have similar charge distributions.

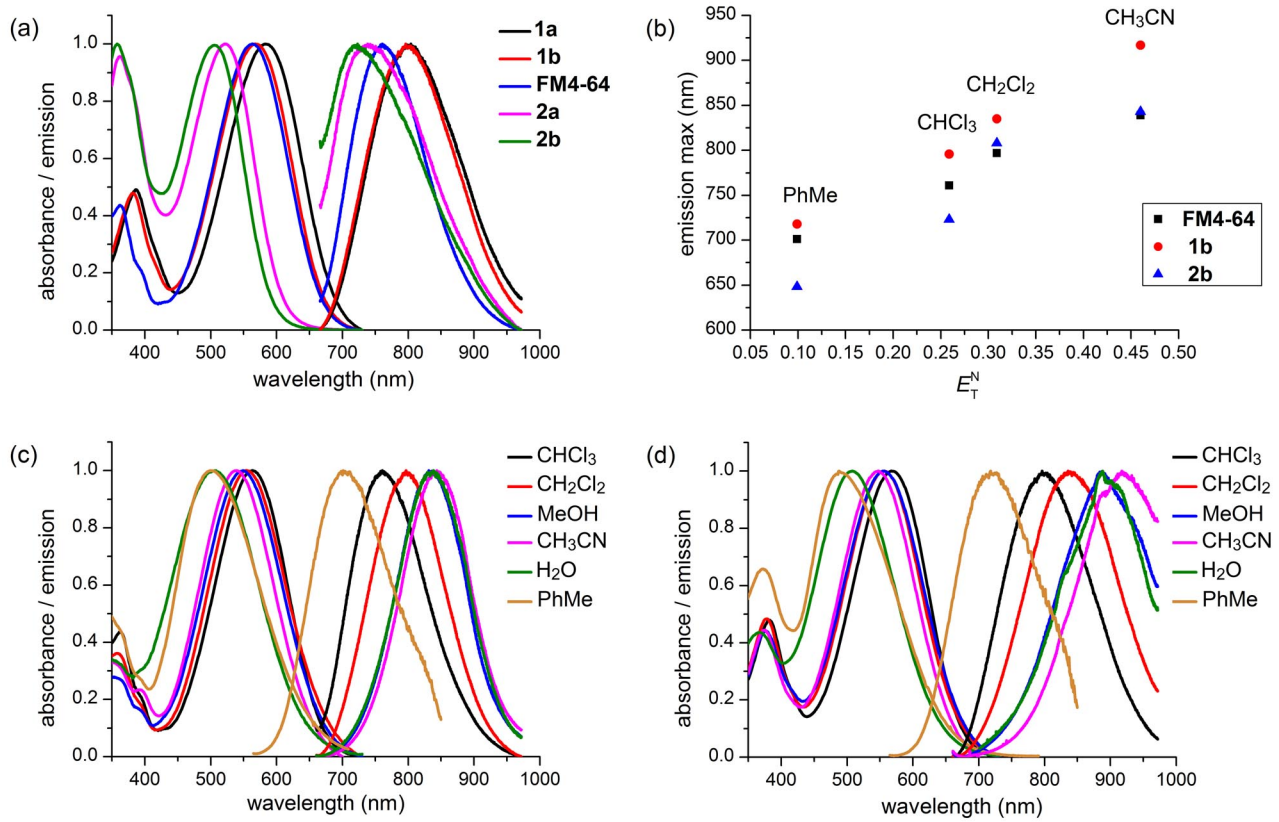

Fig. 1 (a) Normalized absorption and emission spectra for compounds **FM4-64**, **1a,b** and **2a,b** in $CHCl_3$. (b) Plot of emission maxima against the Reichardt E_T parameters.[21] Normalized absorption and emission spectra of **FM4-64** (c) and **1b** (d), in different solvents. All fluorescence spectra were recorded with excitation at the wavelength of maximum absorption.

Table 1 Photophysical properties of the thiophene dyes **1a**, **1b**, **2a** and **2b**, and **FM4-64** in $CHCl_3$.

Dye	ε (λ_{max}^{abs})/10^3 M^{-1} cm^{-1}	λ_{max}^{abs}	λ_{max}^{em}	$\Delta\tilde{\nu}$/cm^{-1}	Φ_F[a]	β_{zzz}/10^{-30} esu[b]	$\beta_{zzz,0}$/10^{-30} esu[c]
FM4-64	48.1	564	761	4590	0.35	840	420
1a	32.0	583	804	4715	0.13	710	370
1b	45.7	568	796	5043	0.25	750	380
2a	45.8	521	738	5644	0.006	390	150
2b	27.5	506	723	5932	0.01	460	160

[a] Fluorescence quantum yields (relative to cresyl violet standard $\Phi = 0.54$), 10% standard error. [b]First hyperpolarizability from HRS at 800 nm; 15% uncertainty. [c] Calculated static first hyperpolarizability, estimated via the two-state model.

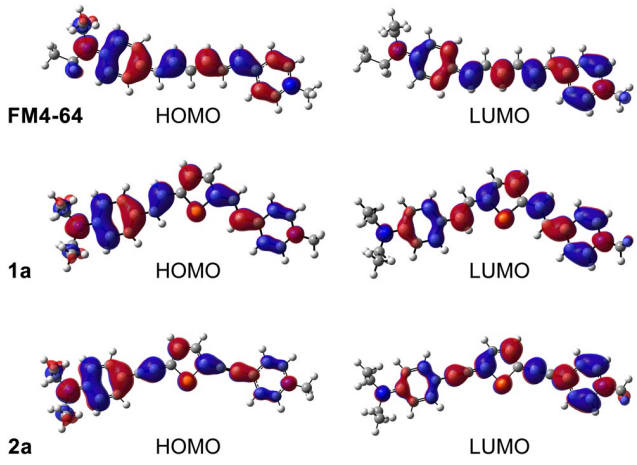

Fig. 2 HOMO and LUMO electron-density isosurfaces illustrating the degree of charge transfer between the ground and 1st excited states of dyes **FM4-64**, **1a** and **2a**.

The investigation of linear optical properties was supplemented by electronic structure calculations, performed using the Gaussian03 software suite. Molecular geometries were optimized *in vacuo* at the DFT level of theory with the B3LYP exchange-correlation potential with the 3-21g basis set. All the calculated geometries have planar π-conjugated frameworks. The optimized geometries were used for ground state energy calculations at the same DFT/B3LYP/3-21g level. Visual inspection of the frontier molecular orbitals shows higher electron density in the HOMO at the donor (-NEt_2) end of the molecules, with the clear reversal of electron density bias towards the acceptor in LUMO (Fig. 2). Since both the HOMOs and the LUMOs are spread over the entire molecular structures, significant HOMO-LUMO overlap is expected, leading to a strongly allowed band with strong charge-transfer character.

Nonlinear Optical Properties

The molecular first hyperpolarizability (β) is a key factor determining the efficiency of SHG in imaging experiments. Hyper-Rayleigh scattering (HRS) was used to measure this parameter for the thiophene-based dyes, **1a,b** and **2a,b**, and benchmark dye **FM4-64**,[23] in chloroform at 800 nm. The β_{zzz} values, which correspond to the diagonal component of the first hyperpolarizability tensor along the dipole moment axis (z), are presented in Table 1. These nonlinear optical data give a similar picture to the linear absorption spectra: vinylene bridges lead to more efficient conjugation and higher β_{zzz} values. For the particular fundamental wavelength used (800 nm), the second-harmonic wavelength (400 nm) is slightly closer to the resonance wavelength for the less conjugated ethynylene-linked chromophores **2a,b**, resulting in a somewhat stronger resonance enhancement for their dynamic β_{zzz} values. An estimate for this enhancement can be derived from the two-level model.[24] The resulting static $\beta_{zzz,0}$ values (Table 1) also show larger hyperpolarizabilities for the vinylene-linked chromophores **1a,b**.

The differences in HRS response between the derivatives **1a,b** and **FM4-64** are not very significant, while the response from **2a,b** is smaller by about a factor of two. As in the case of the linear optical properties, it is apparent that, when comparing **1a,b** and **FM4-64** dyes, the substitution of a –C=C– vinylene unit by a thiophene does not strongly affect the NLO properties. All five dyes have little one-photon absorption beyond 700 nm, and their weak fluorescence, combined with a moderate nonlinear optical response, quantified by the β_{zzz} value, means that once ordered in lipid membranes, the chromophores should give bright SHG images with a low fluorescence background.

Voltage-dependent fluorescence and SHG can be useful for imaging transmembrane potential in neurons and other excitable cells.[3,5,8c] We investigated the voltage sensitivity of the SHG and TPEF of dyes **1b**, **2b** and **FM4-64** in a hemispherical lipid bilayer using our recently reported protocol,[8c] with a lipid bilayer prepared from a solution of diphytanoylphosphatidylcholine (DPhPC, 30 mM) and oxidized cholesterol (5 mM) in dodecane, with excitation at 850 nm (100 fs pulses, 80 MHz repetition rate, simultaneously recording SHG and TPEF). The vinylene-linked dye **1b** showed a TPEF voltage-sensitivity of $\Delta S/S$ = (–7.15 ± 1.33)% per 100 mV which is twice that of **FM4-64** (–3.02 ± 0.02)% per 100 mV). The SHG voltage-sensitivity of **1b** was too weak to measure reliably ($\Delta S/S$ < 1% per 100 mV) and **2b** did not exhibit significant voltage sensitivity in TPEF or SHG.

In Vitro Cytotoxicity

The cytotoxicity of all five dyes was investigated, both in the dark and under visible irradiation, so as to evaluate their suitability for *in vitro* imaging. The dark toxicity of thiophene derivatives, **1a,b** and **2a,b**, and benchmark dye **FM4-64** toward human adherent cervical epithelial carcinoma (HeLa) cells were determined by the MTS tetrazolium (Owen's reagent) assay, after exposure of the cells to the dyes at a range of concentrations for 3 hours (detailed experimental procedure is described in ESI).[25] The results are summarized in Fig. 3a. No significant dark toxicity was observed for **FM4-64**, **1b** and **2b** at concentrations of less than 50 μM. At a dye concentration of 100 μM, **FM4-64** showed a small drop in cell viability (85 ± 18%) and the

thiophene dyes show significant toxicity, with cell viabilities of 60 ± 14% for **1b** and 6 ± 3% for **2b**.

The range of concentrations typically used in cell imaging experiments is 1–10 μM.[8] In this concentration range, both thiophene dyes **1b** and **2b** showed negligible cytotoxicity. On the other hand, singly-charged dyes **1a** and **2a** are lethal, even at low concentrations. This high toxicity appears to be related to the observation that these dyes internalize rapidly into cells, as shown by fluorescence imaging experiments (see below).

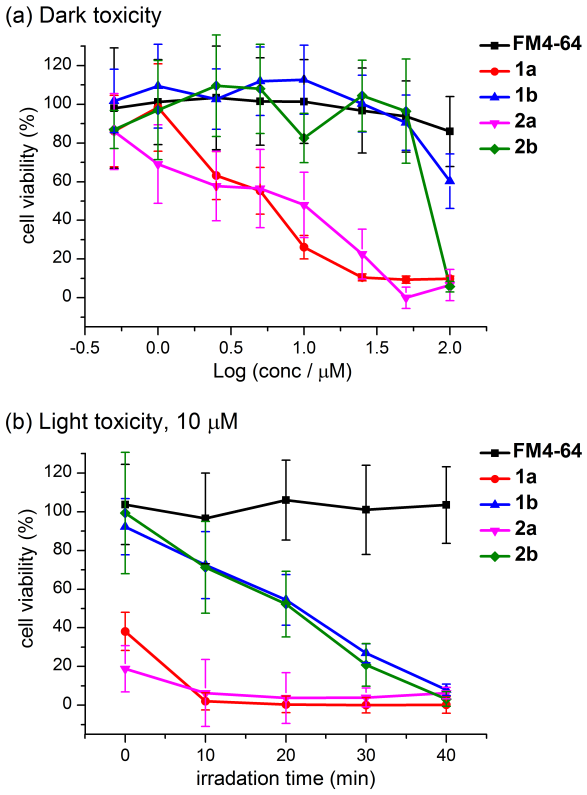

Fig. 3 (a) Viabilities of HeLa cells incubated for 3 h at eight different concentrations (0.5, 1.0, 2.5, 5.0, 10, 25, 50, 100 μM) of **FM4-64** and thiophene-based dyes **1a,b** and **2a,b** in the dark. (b) Viabilities of HeLa cells incubated with 10 μM of **FM4-64** and thiophene-based targets **1a,b** and **2a,b** for 3 h in the dark and then irradiated at 525 nm. Error bars represent ±1 standard deviation.

Phototoxicity experiments were performed by incubating HeLa cells in a solution of each dye at 10 μM concentrations for 3 hours and then irradiating at the wavelength of the main absorption band (LED λ_{max} = 525 nm, FWHM = 32 nm, 0.85 mW, Dotlight, Germany) for 10, 20, 30 and 40 min. The cells were then washed with fresh medium and allowed to grow for another two days before the cell viability was determined, to allow for apoptotic and necrotic responses to irradiation. The results are summarized in Fig. 3b. High phototoxicities were observed for all four thiophene dyes, including **1b** and **2b**, although these compounds are not toxic in the dark. In contrast, **FM4-64** remained non-toxic, with 100% cell survival after 40 min light exposure. These phototoxicity experiments were repeated for **1b** and **2b** at a concentration of 1 μM; under these conditions no significant phototoxicity was detected and the cell viability was 90 ± 10% even after 40 min irradiation. However dye **1a** shows significant phototoxicity, even at a concentration of 0.5 μM, despite showing very little dark toxicity under these dilute conditions.

Fluorescence imaging experiments showed that all the dyes exhibit fast intracellular uptake and internal organelle staining when delivered in standard DMEM medium (faster than 1 min for all dyes at room temperature). The rates of intracellular uptake were fastest with **1a** and **2a**, which exhibit the highest phototoxicity. Even the doubly-charged **1b** and **2b**, which internalize more slowly, show clear phototoxicity upon prolonged laser irradiation in cells on the microscope stage, with **2b** being more phototoxic than **1b**. It has been suggested that the phototoxicity of styryl dyes can be caused by singlet oxygen, an excited state of O_2 produced by energy transfer from the triplet state of the dye to molecular oxygen.[15,26] We investigated the singlet oxygen yields of the dyes by monitoring the emission from singlet oxygen at 1270 nm following excitation of **FM4-64**, **1b** and **2b** in air-saturated acetonitrile solutions. None of the dyes gave any significant signal at 1270 nm (compared to Rose Bengal, a standard singlet oxygen sensitizer, Φ_Δ = 0.74). Therefore, we conclude that singlet oxygen generation by **FM4-64**, **1b** and **2b** is not significant, and that the observed phototoxicity originates from other photochemical processes, i.e. that it is due to the type I rather than the type II chemistry.[27]

The low dark and light toxicities of **1b** and **2b** at 1 μM concentration, combined with their favorable photophysical properties, such as weak fluorescence in polar solvents, make these dyes potential candidates for SHG and fluorescence imaging of membranes. Thus, we decided to focus the linear and nonlinear optical imaging experiments on dyes **1b**, **2b** and **FM4-64**, at a concentration of 1 μM, which is below the toxicity threshold for dark toxicity and phototoxicity.

Fluorescence Imaging

Preliminary imaging with giant unilamellar vesicles (GUVs),[28] showed that all the dyes localize in lipid bilayer membranes, and that they become more fluorescent when they insert into the membrane (Fig. 4). Dyes **1b** and **2b** showed the greatest increase in fluorescence intensity when inserting into the lipid bilayer, giving brighter images than **FM4-64** at identical concentrations. Following this encouraging result, we compared the localization and nonlinear optical imaging behavior of these two dyes, with **FM4-64** as a benchmark. The dyes were tested for wide-field, confocal and multiphoton fluorescence imaging in three different cell types (HeLa, SK-OV-3 and MDA-231) to assess the localization and the increase in fluorescence upon membrane binding. Upon addition of 1 μM dye solutions to cells, the thiophene dyes provide excellent fluorescence images, whereas **FM4-64** does not give good images under the same conditions (Fig. S12). Thus, from the point of view of their photophysical behavior, **1b** and **2b** are superior probes. However, it is worth noting that in order to obtain good contrast images the concentration of **FM4-64** can be easily increased to 10 μM, since it does not pose phototoxicity concerns. Singly-charged thiophene dyes **la** and **2a** showed more intense fluorescence than their doubly-charged analogues; however, their rate of internalization is also greater, as is their phototoxicity.

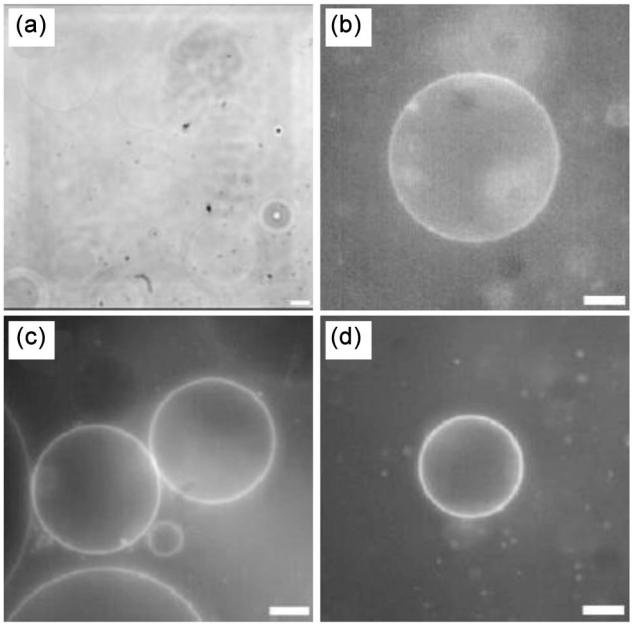

Fig. 4 Wide-field images of GUVs. (a) Bright-field image under white-light illumination of GUVs without any dye and (b)-(d) fluorescence images (excitation: 420 nm) of GUVs stained with 2 μM solutions of (b) **FM4-64**, (c) **1b** and (d) **2b**. Scale bar = 10 μm.

Longer-term localization studies were performed using SK-OV-3 cells. Due to the toxicology profile of the thiophene dyes upon internalization, a method of imaging the cells with the dyes for extended periods of times was developed. Prior to imaging, SK-OV-3 cells were incubated in a 2.5 μM dye solution at 4 °C with Mg^{2+} and Ca^{2+} free medium, in order to prevent endocytosis. Under these conditions, membrane-uptake by the dyes is still fast (Fig. S13), and the dyes remain exclusively in the plasma membranes even after 12 hours of incubation, in contrast to **FM4-64** which is observed in the cytosol and intercellular structures, as shown in Fig. 5.

Fluorescence spectra recorded for **FM4-64**, **1b** and **2b** from membrane regions of SK-OV-3 cells are shown in Fig. 6. Comparison of these emission spectra with those recorded in the series of solvents of varied polarity (Fig. 1) demonstrates that the spectra recorded from cells are significantly blue shifted, indicating that the dyes are in a nonpolar environment. The vinylene-linked thiophene dye **1b** was found to be the most promising fluorescent probe for imaging in cells. In solution, the fluorescence quantum yield of **1b** is 1.5 times less than that of **FM4-64** (Table 1), but upon binding to the cell plasma membrane, it showed a marked increase in fluorescence intensity, resulting in ca. 3 times brighter images for **1b** than for **FM4-64** (Fig. S12).

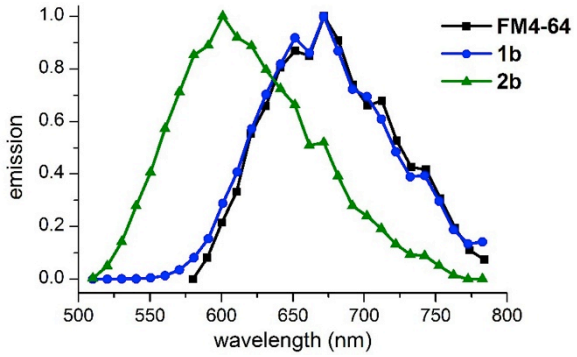

Fig. 6 Emission spectra of **FM4-64**, **1b** and **2b** dyes in live SK-OV-3 cells (excitation: 488 nm).

Nonlinear Optical Imaging of Live Cells

Following successful cellular localization studies, we examined the nonlinear optical imaging properties of non-toxic dyes **1b** and **2b** in living cells through TPEF and SHG imaging. In our confocal scanning multiphoton microscope, a mode-locked Ti:Sapphire laser was tuned to 900 nm and used to scan over the sample, allowing collection of two-photon fluorescence (525 ± 20 nm) in the epi-channel and SHG (450 ± 20 nm) in the transmission channel. The fluorescence and SHG images for **1b** and **FM4-64** are shown in Fig. 7. It is clear that SHG is generated exclusively from the plasma membranes of the cells, where the cell-media boundary provides an asymmetrical environment to order the dye molecules dyes. TPEF does not have this symmetry constraint, so membranes where two cells meet can be seen by TPEF, but not by SHG since local symmetry leads to destructive interference of the SHG signal.[29]

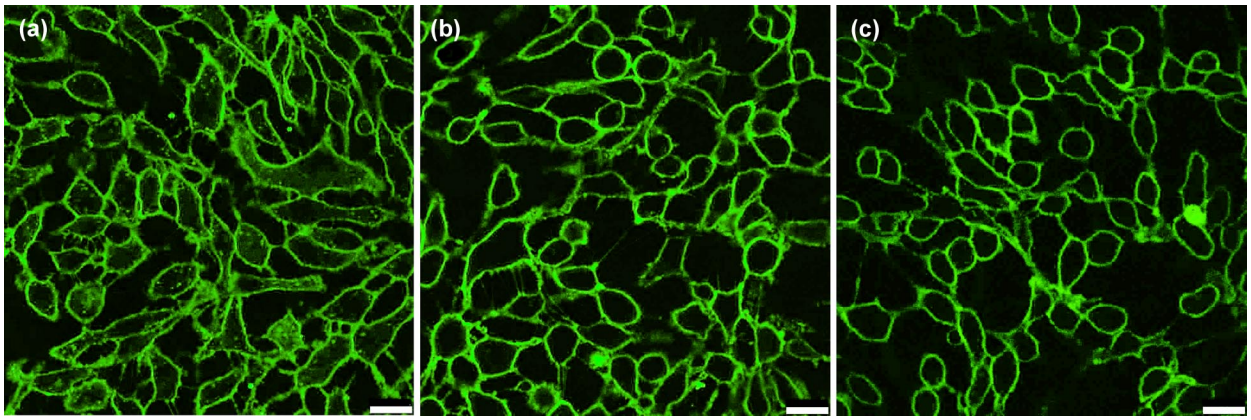

Fig. 5 Normalized confocal laser scanning microscopy images of live SK-OV-3 cells showing localization (green) of dyes (a) **FM4-64**, (b) **1b** and (c) **2b** excited at 488 nm. **FM4-64** shows significantly greater internalization, with appreciable fluorescence from the cytosol and intercellular structures. (Scale bar = 25 μm. SK-OV-3 cells incubated with a 2.5 μM dye solution at 4 °C with Mg^{2+} and Ca^{2+} free medium to prevent endocytosis.)

Cite this: DOI: 10.1039/c0xx00000x

www.rsc.org/xxxxxx

ARTICLE TYPE

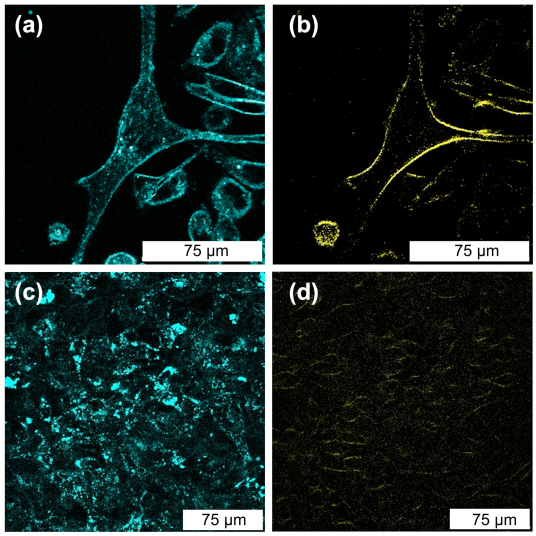

Fig. 7 Scanning confocal multiphoton microscopy images of live MDA-231 cells stained with 2.5 µM PBS solutions of **1b** (a, b) and **FM4-64** (c, d) at 37 °C. Two-photon fluorescence (blue, a and c) and SHG (yellow, b and d) images were recorded using 900 nm excitation. Scale bar = 75 µm.

Interestingly, while the TPEF intensity of **1b** and **FM4-64** in cells is comparable, the SHG signal for the thiophene dye is considerably brighter. The absorption and fluorescence spectra of these two dyes in different solvents (Fig. 1) and in cells (Fig. 6) are nearly identical. Therefore two-photon excitation at the same wavelength should allow direct comparison between the efficiency of these two dyes for nonlinear optical imaging. Our data demonstrate that **1b** and **2b** are more effective as nonlinear imaging agents for live cells than **FM4-64** (Fig. 7 and Fig. S14). One factor responsible for the difference in intensity is a high proportion of internalized **FM4-64**, which reduces the amount of dye in the plasma membrane. However, combined nonlinear imaging data (Fig. 7) and one-photon imaging data (Fig. S12) confirm the superior spectroscopic properties of **1b** and **2b**, resulting in higher fluorescence intensity of these new dyes in cell plasma membranes.

Conclusions

A new family of thiophene dyes **1a/b** and **2a/b** has been synthesized and tested for imaging plasma membranes by TPEF and SHG, in comparison with the commercially available dye **FM4-64**. The synthesis of the vinylene-linked dyes, **1a/b**, by Knoevenagel reaction, is easier than that of the ethynylene-linked dyes, **2a/b**, by Sonogashira coupling and *N*-alkylation. All the dyes exhibit fluorescence in the NIR with strong positive solvatochromism; the emission bands extend to about 900 nm in polar solvents such as water and acetonitrile. The absorption spectra, fluorescence spectra, solvatochromism and hyperpolarizability of the vinylene-linked dyes, **1a/b** are similar to those of **FM4-64**, indicating that replacement of a vinylene-link by a thiophene unit has little effect on the electronic structure. The ethynylene-linked dyes **2a/b** are less π-conjugated than the vinylene-linked dyes, as indicated by blue-shifted absorption and fluorescence spectra, and smaller hyperpolarizabilities.

The toxicity of the dyes is dependent on the type of cationic pyridinium head-group. The singly-charged methyl-pyridinium dyes **1a** and **2a** are toxic to HeLa cells in the dark at concentrations above 1 µM, whereas the dyes with doubly-charged head groups **1b** and **2b** only exhibit dark-toxicity at concentrations above 50 µM. The greater toxicity of the singly-charged methyl-pyridinium compounds, **1a** and **2a**, appears to be related to their rapid internalization into cells. All four thiophene-based dyes show significant phototoxicity at concentrations above 1 µM, however none of them have significant singlet oxygen yields. Under incubation conditions that prevent endocytosis, dyes **1b** and **2b** remained exclusively in the plasma membrane, even 12 h after incubation, whereas **FM4-64** diffuses into in the cytosol and possibly binds to intracellular structures. The low dark- and light-toxicities of **1b** and **2b** at 1 µM concentration, combined with favorable photophysical properties, such as weak fluorescence in polar solvents, make them useful membrane probes for combined second-harmonic and two-photon fluorescence in cellular imaging.

Experimental

NIR Fluorescence Spectra: Room temperature NIR fluorescence spectra were recorded using an automated custom-built system consisting of a 75 W xenon lamp focused into a monochromator and a silicon photodiode used to normalize the incident excitation intensities. Luminescence from the sample was collected at 90° to the excitation beam and focused into a spectrograph fitted with a liquid nitrogen cooled InGaAs photodiode array. The spectral response of the detector was corrected by using a standard tungsten lamp (OL 245U, Optronic Laboratories Inc.).

Preparation of Cell Samples: Cells (HeLa, MDA-231 or SK-OV-3) suspended in a solution of trypsin (3 mL) were quenched with media (3 mL; DMEM, Sigma, 10% FBS, 1% PS, 1% LG) and 10 µL of the solution was placed into a haemocytometer (Neubauer) and counted under magnification. The solution was diluted to obtain a final concentration of 5×10^4 cells, of which 300 µL was added into each well of Lab-Tek Chamber slides (borosilicate glass) for imaging. The wells were incubated for 2 days prior to microscopy studies using 1–10 µM solution of dye in a DMEM medium, which was prepared from a stock solution of the dye in DMSO. For long term localization studies, prior to imaging, cells were incubated in Mg^{2+} and Ca^{2+} free medium, which contained 2.5 µM dye at 4 °C, in order to prevent

endocytosis.

Wide-Field Fluorescence Imaging: The 1 and 10 μM solutions of dye were made up from the addition of a stock of the dye in DMSO (spectroscopic grade, Aldrich, 1 mM) to a solution of HeLa cells in wells. For imaging GUVs, the final concentration of dye was 2 μM. The wells were then left for a few minutes to allow uptake of dye and were then imaged by widefield microscopy (Nikon Eclipse TE2000-S fitted with a Hamamatsu C9100 CCD).

Confocal and Multiphoton Imaging: The confocal images of cells were obtained using inverted scanning confocal microscope TCS SP5, Leica Microsystems Ltd with a 488 nm excitation from an internal Argon ion laser through an x63 (NA 1.2) HCX PL APO CS water immersion objective lens with correction collar (11506279, Leica Microsystems Ltd.). For nonlinear imaging the 900 nm excitation from a Ti-Sapphire pulsed laser source (680–1080 nm, 80 MHz, 140 fs, Chameleon Vision II, Coherent Inc.) was used. SHG signal detection was performed in transmission mode using (450±20 nm) band pass filter, while two-photon fluorescence was collected by a descanned detector using (525±20 nm) band pass filter.

Synthesis: The manipulation of all air- and/or water-sensitive compounds was carried out using standard high vacuum techniques. Dry toluene and dichloromethane were obtained by passing the solvent through activated alumina. Triethylamine and acetonitrile were distilled from CaH_2 under nitrogen before use. Pyridine and pyrrole were distilled from CaH_2 under reduced pressure. All other reagents were used as supplied by commercial agents. Analytical thin layer chromatography (TLC) was carried out on Merck aluminum backed silica gel 60 GF254 plates and visualization when required was achieved using UV light. Column chromatography was carried out on silica gel 60 GF254 using a positive pressure of nitrogen. Where mixtures of solvents were used, ratios reported are by volume. Size-exclusion chromatography was carried out using Bio-Beads S-X1, 200–400 mesh (Bio-Rad). NMR spectra were recorded at the ambient probe temperature using either a Bruker DPX400 (400 MHz), or Bruker AV400 (400 MHz), or Bruker AVII500 (500 MHz). Chemical shifts are quoted as parts per million (ppm) relative to tetramethylsilane and coupling constants (*J*) are quoted in Hertz (Hz). Where assignments of ^{1}H NMR spectra are given, they have been unambiguously established *via* COSY experiments. UV-vis spectra were recorded on a Perkin Elmer Lambda 20 spectrometer. Mass spectra were carried out using Matrix Assisted Laser Desorption Ionization-Time of Flight (MALDI-TOF) only molecular ions and major peaks are reported. HPLC analysis were carried out on a HitaChrom ELITE HPLC system equipped with L-2130 quaternary pump, L-2455 diode array detector, L-2200 autosampler, L-2350 column oven and Foxy Jr. fraction collector. Analytical HPLC was carried out using C8 5 mm, 3.9 × 150 mm Eclipse XDB-C8 column (Agilent) using 1 mL min^{-1} flow and a stepwise gradient at 40 °C. The chromatographic separations were monitored in the range 260–800 nm. The synthesis and characterization of compounds **3**, **4a,b** and **5** are described in the Supplementary Information.

4-((*E*)-2-{5-[(*E*)-4-(Diethylamino)styryl]thiophen-2-yl}vinyl)-1-methylpyridin-1-ium chloride 1a. 5-{(*E*)-2-[4-(Diethylamino)phenyl]ethenyl}thiophene-2-carboxaldehyde **3** (291 mg, 1.02 mmol), 1,4-dimethylpyridin-1-ium iodide **4a** (200 mg, 0.85 mmol), pyrrolidine (0.85 mL), and EtOH (30 mL) were stirred at room temperature overnight. The solution turned purple during the reaction. The mixture was evaporated and the crude product was recrystallized by dissolving in a small amount of $CHCl_3$ followed by layered addition of a large volume of toluene, then allowing to stand at 4 °C overnight. The precipitate was filtered off and ion-exchanged by dissolving in a small volume of methanol followed by addition of saturated aqueous brine and extraction into $CHCl_3$ to give dye **1a** as a dark purple solid; yield 430 mg (81%). λ_{max} (CH_2Cl_2)/ nm (log ε) 385 (4.21), 579 (4.49); m.p. 206–208 °C; ^{1}H NMR (400 MHz, CD_3OD) δ_H 1.20 (t, *J* = 7.0 Hz, 6H), 3.45 (q, *J* = 7.0 Hz, 4H) 4.26 (s, 3H), 6.72 (t, *J* = 8.3 Hz, 2H), 7.00 (d, *J* = 16.3 Hz, 2H), 7.07 (d, *J* = 3.9 Hz, 1H), 7.10 (d, *J* = 16.3 Hz, 1H), 7.38 (d, *J* = 3.9 Hz, 2H), 7.40 (d, *J* = 8.3 Hz, 2H), 8.03 (d, *J* = 6.5 Hz, 2H), 8.06 (d, *J* = 15.6 Hz, 1H), 8.59 (d, *J* = 6.5 Hz, 2H); ^{13}C NMR (100 MHz, CD_3OD) δ_C 21.99, 53.19, 56.09, 120.88, 125.48, 130.14, 132.24, 132.32, 135.86, 137.92, 140.89, 143.16, 143.42, 147.07, 154.17, 157.15, 157.62, 161.70, 162.70, 163.34; HRMS (ESI) *m/z* 375.1886 ($C_{24}H_{27}N_2S$, M^+, requires 375.1889, 100%).

4-((*E*)-2-{5-[(*E*)-4-(Diethylamino)styryl]thiophen-2-yl}vinyl)-1-[3-(triethylammonio)propyl]pyridin-1-ium chloride 1b. 5-{(*E*)-2-[4-(Diethylamino)phenyl]ethenyl}thiophene-2-carboxaldehyde **3** (150 mg, 0.526 mmol), 4-methyl-1-[3-(triethylammonio)propyl]pyridin-1-ium chloride **4b** (215 mg, 0.438 mmol), pyrrolidine (0.44 mL), and EtOH (20 mL) were stirred at room temperature overnight. The solution turned purple during the reaction. The solvent was then evaporated under vacuum at 30 °C. The residue was purified by a column chromatography (SiO_2, 9:1 $CHCl_3$:MeOH then 7:2:1 MeOH:NH_4Cl [aq. 0.4 M]:$MeNO_2$). Further purification was performed using size exclusion chromatography ($CHCl_3$). The crude product was precipitated by dissolving it in a small amount of $CHCl_3$ followed by layered addition of a large volume of hexane. The resulting solution was kept at 4 °C overnight. Dye **1b** was filtered off as a dark purple solid; yield 135 mg (45%). λ_{max} (CH_2Cl_2)/ nm (log ε) 378 (4.39), 555 (4.70); m.p. > 250 °C; ^{1}H NMR (400 MHz, CD_3OD) δ_H 1.18 (t, *J* = 7.0 Hz, 6H), 1.34 (t, *J* = 7.3 Hz, 9H), 2.39-2.51 (m, 2H), 3.34-3.48 (m, 12H), 4.59 (t, *J* = 7.7 Hz, 2H), 6.72 (d, *J* = 7.7 Hz, 2H), 6.98 (d, *J* = 16.5 Hz, 2H), 7.06 (d, *J* = 3.5 Hz, 1H), 7.08 (d, *J* = 16.5 Hz, 1H), 7.38 (d, *J* = 3.5 Hz, 2H), 7.39 (d, *J* = 7.7 Hz, 2H), 8.06 (d, *J* = 6.7 Hz, 2H), 8.07 (d, *J* = 16.5 Hz, 1H), 8.80 (d, *J* = 6.7 Hz, 2H); ^{13}C NMR (125 MHz, CD_3OD) δ_C 7.80, 12.98, 19.33, 24.96, 45.69, 54.39, 57.69, 113.22, 117.31, 121,13, 124.49, 125.28, 127.44, 128.54, 129.58, 133.39, 135.68, 136.54, 139.25, 145.17, 151.31, 155.76; HRMS (ESI) *m/z* 538.3019 ($C_{32}H_{45}ClN_3S$, $[M+Cl]^+$, requires 538.3017, 100%); Analysis found (calcd $C_{32}H_{45}Cl_2N_3S$): C, 66.66 (66.88); H, 7.62 (7.89); N, 7.14 (7.31) %.

***N,N*-Diethyl-4-{[5-(pyridin-4-yl)thiophen-2-yl]ethynyl} aniline 6.** *N,N*-Diethyl-4-((5-((trimethylsilyl)ethynyl)thiophen-2-yl)ethynyl)aniline **5** (475 mg, 1.35 mmol) was stirred with a solution of K_2CO_3 (933 mg, 6.75 mmol) in THF (15 mL) and MeOH (5 mL) overnight under nitrogen. The mixture was diluted

with hexane (100 mL) and washed with distilled water (3 × 50 mL). The organic layer was dried over anhydrous $MgSO_4$ and the solvents were evaporated. The crude product, obtained as a colorless oil, was used in the next step without further purification. Thus, the corresponding *N,N*-diethyl-4-((5-ethynyl thiophen-2-yl)ethynyl)aniline (378 mg, 1.35 mmol) was dissolved in a mixture of toluene (5 mL) and diisopropylamine (2 mL) and the solution was degassed by three freeze-thaw cycles. 4-Iodopyridine (830 mg, 4.05 mmol), tris(dibenzylideneacetone)dipalladium (62.3 mg, 68.0 µmol), triphenylphosphine (70.8 mg, 270 µmol) and copper(I) iodide (25.7 mg, 135 µmol) were then added. The mixture was stirred at room temperature for 30 min. The product precipitated out. The mixture was then diluted with CH_2Cl_2 (50 mL) and washed with distilled water (50 mL), saturated aqueous NH_4Cl (50 mL) and distilled water (50 mL). The organic layer was dried over anhydrous $MgSO_4$ and the solvents were removed by rotary evaporation. The crude product was further purified by column chromatography (SiO_2, 3:1 $CHCl_3$:Et_2O). Compound **6** was obtained as a dark yellow solid. Yield 418 mg (87%). λ_{max} (DMF)/ nm (log ε) 320 (4.42) 400 (4.54); m.p. 141–143 °C; ^{1}H NMR (400 MHz, $CDCl_3$) δ_H 1.19 (t, J = 7.1 Hz, 6H), 3.39 (q, J = 7.1 Hz, 4H), 6.62 (d, J = 8.9 Hz, 2H), 7.09 (d, J = 3.9 Hz, 1H), 7.21 (d, J = 3.9 Hz, 1H), 7.36 (d, J = 4.8 Hz, 2H), 7.37 (d, J = 8.3 Hz, 2H), 8.61 (d, J = 4.8 Hz, 2H); ^{13}C NMR (100 MHz, $CDCl_3$) δ_C 12.54, 44.35, 79.91, 87.34, 90.83, 96.82, 107.64, 111.12, 121.58, 125.11, 127.76, 130.58, 130.98, 133.00, 133.25, 147.94, 149.76; MS (ESI) *m/z* 356.1341 ($C_{23}H_{20}N_2S$, $[M]^+$, requires 356.1347, 100%).

4-[(5-{[4-(Diethylamino)phenyl]ethynyl} thiophen-2-yl) ethynyl]-1-methylpyridin-1-ium chloride 2a. *N,N*-Diethyl-4-((5-(pyridin-4-yl)thiophen-2-yl)ethynyl) aniline **6** (50.0 mg, 140 µmol) was dissolved in THF (1.0 mL) and methyl iodide (1.25 mL, 20.0 mmol). The solution was stirred at room temperature for 24 h, then evaporated. The crude product was passed through a Dowex 1x8 200 mesh ion-exchange column (DMF). The product was precipitated by dissolving it in a small amount of $CHCl_3$ followed by layered addition of a large volume of petroleum ether (40–60 °C). The resulting solution was kept at 4 °C overnight. Dye **2a** was filtered off as a dark red solid. Yield 61 mg (88%). λ_{max} (CH_2Cl_2)/ nm (log ε) 362 (4.71), 520 (4.72); m.p. 226–228 °C; ^{1}H NMR (400 MHz, $CDCl_3$) δ_H 1.19 (t, J = 7.1 Hz, 6H), 3.39 (q, J = 7.1 Hz, 4H), 6.62 (d, J = 8.9 Hz, 2H), 7.09 (d, J = 3.9 Hz, 1H), 7.21 (d, J = 3.9 Hz, 1H), 7.36 (d, J = 4.8 Hz, 2H), 7.37 (d, J = 8.3 Hz, 2H), 8.61 (d, J = 4.8 Hz, 2H); ^{13}C NMR (100 MHz, $CDCl_3$ + CD_3OD) δ_C 12.04, 44.04, 79.64, 86.86, 89.86, 96.35, 99.22, 106.64, 110.90, 118.59, 128.13, 130.72, 131.54, 132.83, 126.65, 139.83, 144.55, 148.00; HRMS (ESI) *m/z* 371.1576 ($C_{24}H_{23}N_2S$, M^+, requires 371.1576, 100%); Analysis found (calcd $C_{24}H_{23}ClN_2S$): C, 57.82 (57.83); H, 4.58 (4.65); N, 5.67 (5.62) %.

4-[(5-{[4-(Diethylamino)phenyl]ethynyl}thiophen-2-yl) ethynyl]-1-[5-(triethylammonio)propyl]pyridin-1-ium chloride 2b. *N,N*-Diethyl-4-((5-(pyridin-4-yl)thiophen-2-yl)ethynyl)aniline **6** (50.0 mg, 0.14 mmol) and (3-iodopropyl)triethylammonium iodide (1.11 g, 2.80 mmol) were dissolved in a mixture of DMSO (6 mL) and benzonitrile (3 mL) and stirred at 75 °C for 1.5 h. The reaction was stopped before completion and the mixture was dried by rotary evaporation. The residue was purified by a column chromatography (SiO_2, gradient of MeOH in $CHCl_3$ to neat MeOH followed by 7:2:1 MeOH:NH_4Cl (aq 0.2 M):$MeNO_2$, and finally by NH_4Cl (aq 0.4 M) to wash off the product). Then, MeOH was removed by rotary evaporation at 35 °C. The residue was then extracted with $CHCl_3$ and precipitated by layered addition of toluene. The resulting solution was kept at 4 °C overnight. Dye **2b** was filtered off as a red tacky solid. Yield 29.0 mg (36%). λ_{max} (CH_2Cl_2)/ nm (log ε) 354 (4.41), 491 (4.44); ^{1}H NMR (400 MHz, CD_3CN) δ_H 1.13 (t, J = 6.9 Hz, 6H), 1.29 (t, J = 7.2 Hz, 9H), 2.50 (m, 2H), 3.29 (q, J = 7.3 Hz, 6H), 3.39 (q, J = 6.9 Hz, 4H), 3.50 (t, J = 8.4 Hz, 2H), 4.96 (t, J = 7.8 Hz, 2H), 6.67 (d, J = 9.0 Hz, 2H), 7.20 (d, J = 3.9 Hz, 1H), 7.33 (d, J = 9.0 Hz, 2H), 7.51 (d, J = 3.9 Hz, 1H), 8.00 (d, J = 6.7 Hz, 2H), 9.51 (d, J = 6.7 Hz, 2H); ^{13}C NMR (125 MHz, $CDCl_3$ + CD_3CN) δ_C 7.42, 11.98, 24.90, 43.87, 53.26, 53.65, 56.60, 79.52, 89.87, 98.42, 98.87, 106.39, 110.69, 118.63, 127.92, 130.56, 131.03, 132.67, 136.40, 139.65, 144.93, 147.81; HRMS (ESI) *m/z* 534.2696 ($C_{32}H_{41}ClN_3S$, $[M+Cl]^+$, requires 534.2704, 100%).

Acknowledgements

We gratefully acknowledge financial support from the EPSRC, including Career Acceleration Fellowship to M.K.K. This work was partially supported by the European Commission in the form of a Marie Curie individual Fellowship to I.L.D. under the contract PIEF-GA-2009-255164. J.P.M. acknowledges the K. U. Leuven IDO project 3E090505.

Notes and references

[a] *Department of Chemistry, Oxford University, Chemistry Research Laboratory, Oxford, UK OX1 3TA, harry.anderson@chem.ox.ac.uk*
[b] *Chemistry Department, Imperial College London, Exhibition Road, London, UK SW7 2AZ. E-mail: m.kuimova@imperial.ac.uk*
[c] *Department of Chemistry, University of Leuven, Celestijnenlaan 200 D, 3001 Leuven, Belgium. E-mail: koen.clays@fys.kuleuven.be*
[d] *Department of Physics, Oxford University, Clarendon Laboratory, Oxford, UK OX1 3PU.*

† Electronic Supplementary Information (ESI) available: Synthetic procedures, spectroscopic data, photophysical characterization and procedures for toxicity experiments. See DOI: 10.1039/b000000x/

1 (a) R. P. Haugland, *The Handbook—A Guide to Fluorescent Probes and Labeling Technologies*, 11th edn. Invitrogen Corp, Carlsbad, 2010; (b) J. Jiang and R. Yuste, *Microscopy and Microanalysis*, 2008, **14**, 526-531.
2 M. Hof, R. Hutterer and V. Fidler, *Fluorescence Spectroscopy in Biology Advanced Methods and their Applications to Membranes, Proteins, DNA, and Cells*, Vol. 3, Springer, Berlin, 2004.
3 (a) R. Yuste, *Nat. Methods*, 2005, **2**, 902-904; (b) J. Mertz, *Curr. Opt. Neurobiol*., 2004, **14**, 610-616; (c) P. J. Campagnola and L. M. Loew, *Nat. Biotechnol*., 2003, **21**, 1356-1360; (d) S. Yao and K. D. Belfield, *Eur. J. Org. Chem*., 2012, 3199-3217.
4 (a) P. J. Campagnola, A. C. Millard, M. Terasaki, P. E. Hoppe, C. J. Malone and W. A. Mohler, *Biophys. J.*, 2002, **82**, 493-508. (b) J. Jiang, K. B. Eisenthal and R. Yuste, *Biophys. J*., 2007, **93**, L26-L28.
5 J. E. Reeve, H. L. Anderson and K. Clays, *Phys. Chem. Chem. Phys.*, 2010, **12**,13484-13498.
6 (a) V. Alain, M. Blanchard-Desce, I. Ledoux-Rak and J. Zyss, *Chem. Commun.*, 2000, 353-354; (b) M. Blanchard-Desce, V. Alain, P. V. Bedworth, S. R. Marder, A. Fort, C. Runser, M. Barzoukas, S. Lebus and R. Wortmann, *Chem. Eur. J.*, 1997, **3**, 1091-1104.

7 J. P. Wuskell, D. Boudreau, M.-d. Wei, L. Jin, R. Engl, R. Chebolu, A. Bullen, K. D. Hoffacker, J. Kerimo, L. B. Cohen, M. R. Zochowski and L. M. Loew, *J. Neurosci. Methods,* 2006, **151**, 200-215.

8 (a) J. E. Reeve, H. A. Collins, K. De Mey, M. M. Kohl, K. J. Thorley, O. Paulsen, K. Clays and H. L. Anderson, *J. Am. Chem. Soc.,* 2009, **131**, 2758-2759; (b) I. López-Duarte, J. E. Reeve, J. Pérez-Moreno, I Boczarow, G. Depotter, J. Fleischhauer, K. Clays and H. L. Anderson, *Chem. Sci.*, 2013, **4**, 2024–2027; (c) J. E. Reeve, A. D. Corbett, I. Boczarow, W. Kaluza, W. Barford, H. Bayley, T. Wilson and H. L. Anderson, *Angew. Chem. Int. Ed.*, 2013, **52**, 9044-9048.

9 (a) C. Barsu, R. Cheaib, S. Chambert, Y. Queneau, O. Maury, D. Cottet, H. Wege, J. Douady, Y. Bretonnière and C. Andraud, *Org. Biomol. Chem.,* 2010, **8**, 142-150; (b) C. Barsu, R. Fortrie, K. Nowika, P. L. Baldeck, J.-C. Vial, A. Barsella, A. Fort, M. Hissler, Y. Bretonnière, O. Maury and C. Andraud, *Chem. Commun.,* 2006, 4744-4746.

10 P. Hrobárik, I. Sigmundová, P. Zahradník, P. Kasák, V. Arion, E. Franz and K. Clays, *J. Phys. Chem. C*, 2010, **114**, 22289-22302.

11 E. De Meulenaere, W.-Q. Chen, S. Van Cleuvenbergen, M.-L. Zheng, S. Psilodimitrakopoulos, R. Paesen, J.-M. Taymans, M. Ameloot, J. Vanderleyden, P. Loza-Alvarez, X.-M. Duan and K. Clays, *Chem. Sci.*, 2012, **3**, 984-995.

12 M. J. Cho, D. H. Choi, P. A. Sullivan, A. J. P. Akelaitis and L. R. Dalton, *Prog. Polym. Sci.*, 2008, **33**, 1013-1058.

13 (a) J.-M. Raimundo, P. Blanchard, N. Gallego-Planas, N. Mercier, I. Ledoux-Rak, R. Hierle and J. Roncali, *J. Org. Chem.,* 2002, **67**, 205-218; (b) A. Mishra, C.-Q. Ma and P. Bäuerle, *Chem. Rev*., 2009, **109**, 1141-1276.

14 (a) M. J. Patrick, L. A. Ernst, A. S. Waggoner, D. Thai, D. Tai and G. Salama, *Org. Biomol. Chem.* 2007, **5**, 3347-3353. (b) P. Yan, A. Xie, M. Wei and L. M. Loew, *J. Org. Chem.,* 2008, **73**, 6587-6594. (c) G. Sotgiu, M. Galeotti, C. Samorí, A. Bongini and A. Mazzanti, *Chem. Eur. J.,* 2011, **17**, 7947-7952; (d) A. Fin, A. Vargas Jentzsch, N. Sakai and S. Matile, *Angew. Chem. Int. Ed.*, 2012, **51**, 12736-12739.

15 (a) W. J. Betz, F. Mao and G. S. Bewick, *J. Neurosci.*, 1992, **12**, 363-375; (b) W. J. Betz, F. Mao and C. B. Smith, *Curr. Opin. Neurobiol.*, 1996, **6**, 365-371.

16 (a) A. J. Cochilla, J. K. Angleson and W. J. Betz, *Annu. Rev. Neurosci.,* 1999, **22**, 1-10; (b) S. Bolte, C. Talbot, Y. Boutte, O. Catrice, N. D. Read and B. Satiat-Jeunemaitre, *J. Microsc.*, 2004, **214**, 159-173.

17 (a) O. Bouevitch, A. Lewis, I. Pinevsky, J. P. Wuskell and L. M. Loew, *Biophys. J.,* 1993, **65**, 672-679; (b) D. A. Dombeck, L. Sacconi, M. Blanchard-Desce and W. W. Webb, *J. Neurophysiol.*, 2005, **94**, 3628-3636; (c) M. Nuriya, J. Jiang, B. Nemet, K. B. Eisenthal and R. Yuste, *Proc. Natl. Acad. Sci. U. S. A.*, 2006, **103**, 786-790.

18 S. J. Loeb and D. A. Tramontozzi, *Org. Biomol. Chem.,* 2005, **3**, 1393-1401.

19 I. Johnson, *Practical considerations in the selection and application of fluorescent probes In Handbook of Biological Confocal Microscopy*. J. B. Pawley, editor. Springer-Verlag New York, Inc., New York, 2006, 353.

20 (a) S.-H. Son, Y. Yamagishi, M. Tani, M. Yuasa and K. Yamada, *Chem. Lett.,* 2011, **40**, 989-991; (b) Y. Wu, F. L. Yeh, F. Mao and E. R. Chapman, *Biophys. J.*, 2009, **97**, 101-109.

21 (a) U. Narang, C. F. Zhao, J. D. Bhawalkar, F. V. Bright and P. N. Prasad, *J. Phys. Chem.,* 1996, **100**, 4521-4525; (b) S. T. Abdel-Halim and M. K. Awad, *J. Mol. Struct.* 2009, **920**, 3321–341.

22 (a) C. Reichardt, *Chem. Rev.*, 1994, **94**, 2319-2358; (b) J. R. Lakowicz, *Principles of Fluorescence Spectroscopy*, 2nd edn, Academic/Plenum, New York, 1999, 205.

23 (a) G. Olbrechts, R. Strobbe, K. Clays and A. Persoons, *Rev. Sci. Instrum.*, 1998, **69**, 2233-2241; (b) B. J. Coe, J. A. Harris, J. J. Hall, B. S. Brunschwig, S.-T. Hung, W. Libaers, K. Clays, S. J. Coles, P. N. Horten, M. E. Light, M. B. Hursthouse, J. Garín and J. Orduna, *Chem. Mater.,* 2006, **18**, 5907-5918.

24 J. L. Oudar and D. S. Chemla, *J. Chem. Phys*., 1977, **66**, 2664-2668.

25 M. V. Berridge and A. S. Tan, *Arch. Biochem. Biophys.,* 1993, **303**, 474-482.

26 B. M. Salzberg, A. L. Obaid, D. M. Senseman and H. Gainer, *Nature*, 1983, **306**, 36-40.

27 E. D. Sternberg, D. Dolphin and C. Brückner, *Tetrahedron*, 1998, **54**, 4151–4202.

28 M. I. Angelova, S. Soleau, P. Meleard, J. F. Faucon and P. Bothorel, in *Trends in Colloid and Interface Science VI, Vol. 89* (Eds.: C. Helm, M. Losche, H. Mohwald), 1992.

29 P. Yan, A. C. Millard, M. Wei and L. M. Loew, *J. Am. Chem. Soc.*, 2006, **128**, 11030-11031.